Echoes of the Electroweak Phase Transition: Discovering a Second Higgs Doublet through $A_0 \to ZH_0$

G. C. Dorsch, S. J. Huber, K. Mimasu, and J. M. No
Department of Physics and Astronomy, University of Sussex, BN1 9QH Brighton, United Kingdom
(Received 7 June 2014; revised manuscript received 22 September 2014; published 20 November 2014)

The existence of a second Higgs doublet in nature could lead to a cosmological first-order electroweak phase transition and explain the origin of the matter-antimatter asymmetry in the Universe. We obtain the spectrum and properties of the new scalars H_0, A_0, and $H^\pm$ that signal such a phase transition and show that the observation of the decay $A_0 \to ZH_0$ at LHC would be a "smoking gun" signature of these scenarios. We analyze the LHC search prospects for this decay in the $\ell\ell b\bar{b}$ and $\ell\ell W^+W^-$ final states, arguing that current data may be sensitive to this signature in the former channel as well as there being great potential for a discovery in either channel at the very early stages of the 14 TeV run.

DOI: 10.1103/PhysRevLett.113.211802 PACS numbers: 12.60.Fr, 14.80.Ec, 98.80.Cq

A key goal of the Large Hadron Collider (LHC) physics program is to reveal the structure of the sector responsible for electroweak symmetry breaking. While ongoing analyses show that the properties of the newly discovered Higgs particle [1,2] are close to those expected for the standard model (SM) Higgs boson h, whether or not the scalar sector has a richer structure, containing additional states, remains an interesting possibility. Scenarios with extra scalar doublets are very well motivated, naturally arising both in weakly coupled completions of the SM, like the minimal supersymmetric standard model (MSSM) [3] and its extensions, and in strongly coupled ones, such as composite Higgs scenarios [4,5]. Moreover, simple extensions of the SM scalar sector, like two-Higgs-doublet models (2HDMs), could address an important open question at the interface of particle physics and cosmology, namely, the generation of the cosmic matter-antimatter asymmetry, via electroweak baryogenesis [6–10] (see also Ref. [11]).

The implications of 2HDMs for electroweak physics and LHC searches have been widely studied (see, e.g., Refs. [12–21]). The mass spectrum of the new states S_i, a charged scalar $H^\pm$ and two neutral scalars H_0, A_0, has a big impact on LHC searches for the second Higgs doublet. In the MSSM, and generically in 2HDMs arising from weakly coupled scenarios, the mass splittings Δm_i among these scalars are small, $\Delta m_i \ll v$, with $v = 246$ GeV the electroweak (EW) scale. The heavier the new scalar states, the more compressed their mass spectrum. For the MSSM the splittings Δm_i are smaller than the mass of the EW gauge bosons, and the decays $S_i \to ZS_j$ or $S_i \to W^\pm S_j$ are not kinematically allowed. Observing such decays at the LHC would point to a very different 2HDM. However, while these decays have already been considered [19,21], such scenarios remain largely unexplored and are not currently part of the main LHC search program.

In this Letter we show that the decay $A_0 \to ZH_0$ is the signature of a strongly first-order electroweak phase transition (EWPT) in 2HDMs, as needed for electroweak baryogenesis. We then show that, while current 2HDM searches by ATLAS and CMS Collaborations are not tailored to probing these scenarios, searches for the decay $A_0 \to ZH_0$ are promising at the 14 TeV run of LHC in the $\ell\ell b\bar{b}$ and $\ell\ell W^+W^-$ channels. This signature therefore provides a connection between the generation of the cosmic matter-antimatter asymmetry and searches for new physics at the LHC.

2HDMs and the electroweak phase transition.—The scalar sector of a 2HDM contains two scalar doublets $\Phi_{1,2}$, its physical spectrum consisting of a charged Higgs $H^\pm$, two charge-parity- (CP)even scalars h and H_0, and a CP-odd scalar A_0 (we assume, for simplicity, no CP violation in the scalar sector). We identify the lightest CP-even Higgs boson h with the scalar resonance recently observed at the LHC, fixing $m_h = 125$ GeV. The remaining parameters in the scalar potential are the masses m_{H_0}, m_{A_0}, $m_{H^\pm}$, two angles β and α, the former defining the ratio of vacuum expectation values (VEVs) of the two doublets $v_{1,2}$ (with $v_1^2 + v_2^2 = v^2$) and the latter characterizing mixing between CP-even states, and a dimensionful parameter μ (for a review of 2HDMs, see, e.g., Ref. [12]). We define α such that, when $\alpha = \beta$, the state H_0 decouples from gauge bosons, and h has SM-like properties (the alignment limit; see Ref. [22] for more details).

The existence of two scalar doublets $\Phi_{1,2}$ coupling to fermions opens an undesirable window for tree-level flavor changing neutral currents. This can be avoided by imposing a Z_2 symmetry, softly broken by the μ parameter in the scalar potential, forcing each fermion type to couple to one doublet only [23]. By convention, up-type quarks couple to the second doublet, but which doublet couples to leptons and down-type quarks may vary. We will focus here on the

type I model, in which all fermions couple to the same doublet. Another scenario is the type II model, where down-type quarks and leptons couple to a different doublet from up-type quarks, and of which the scalar sector of the MSSM is a particular instance. We note that the Z_2 symmetry also forbids quartic scalar potential terms with an odd number of each doublet $\Phi_{1,2}$.

In order to study the strength of the EWPT in 2HDMs, we perform a Monte Carlo scan over m_{H_0}, m_{A_0}, $m_{H^\pm}$, $\tan\beta$, $\alpha-\beta$, and μ using a numerical routine developed in Ref. [22]. The code is interfaced with 2HDMC [24] and HIGGSBOUNDS [25] to select points satisfying unitarity (see Ref. [26]), perturbativity, EW precision constraints, and collider bounds. Stability of the potential is checked at 1-loop by requiring that the EW minimum be the deepest of the effective potential [22]. For the type I model the only relevant flavor constraint comes from $b \to s\gamma$, which we take into account (the points excluded by other constraints, in particular, $B^0 - \bar{B}^0$ mixing and $Z \to b\bar{b}$, are also excluded by $b \to s\gamma$) [27]. The measured properties of h also impose further constraints on $\tan\beta$ and $\alpha-\beta$ (see, e.g., Ref. [16]). While the type of 2HDM considered is irrelevant for the EWPT (since the top coupling is always the same), it does affect experimental constraints. We choose a type I 2HDM, which is less constrained than type II.

A point satisfying the above constraints is deemed *physical*. For each of them, the strength of the EWPT is computed via the thermal 1-loop effective potential by increasing the temperature until the potential has two degenerate minima, which defines the critical temperature T_c. The phase transition is considered strong when $v_c/T_c \geq 1$ [28,29], with v_c the magnitude of the VEV at T_c (see Ref. [22] for details). We find a 1-loop analysis accurate enough for the scope of the present work. While we expect 2-loop corrections to have some quantitative impact [30,31], they should not change the qualitative picture described in the following.

Figure 1 shows heat maps of physical points (left) and points with a strongly first-order EWPT (right) in the planes $(m_{H_0}, \alpha-\beta)$ and (m_{H_0}, m_{A_0}). Altogether, a strong EWPT favors a SM-like light Higgs state h (thus, 2HDMs with a strong EWPT also satisfy type II constraints), i.e., small $\alpha-\beta$ and moderate $\tan\beta$ [22,32]. The viable range of $\alpha-\beta$ shrinks as H_0 becomes heavier since, away from the alignment limit, both h and H_0 "share" the VEV v and the EWPT becomes weaker as the participating states get heavier (see, e.g., Ref. [29]). Figure 1 also shows that a strong EWPT in 2HDMs strongly favors a rather heavy CP-odd scalar state A_0 ($m_{A_0} > 300$ GeV) and a large mass splitting $m_{A_0} - m_{H_0} \gtrsim v$. These results point towards the $A_0 \to ZH_0$ decay channel as a "smoking gun" signature of 2HDMs with a strong EWPT.

The decay $A_0 \to ZH_0$.—Current 2HDM searches at LHC are mainly motivated by the MSSM, where scalar mass splittings are small. The decays $S_i \to ZS_j$ (for

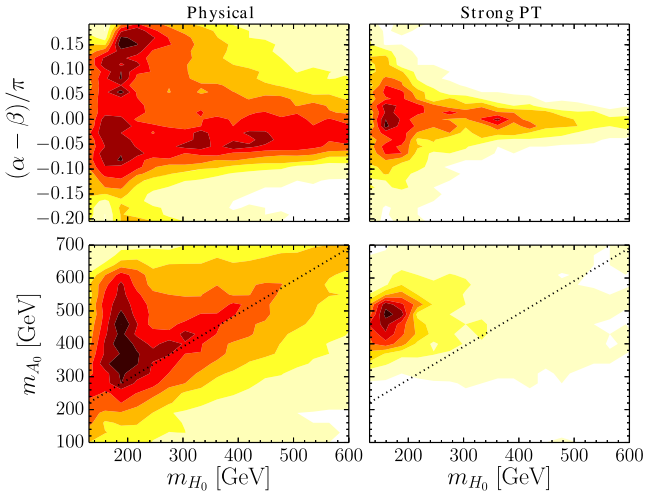

FIG. 1 (color online). Heat maps for the physical region (left) and the region with a strongly first-order EWPT (right). Top: $(m_{H_0}, \alpha-\beta)$ plane. Bottom: (m_{H_0}, m_{A_0}) plane. The dotted black line corresponds to $m_{A_0} = m_{H_0} + m_Z$.

$S_i \in H_0, A_0$) are kinematically forbidden and ATLAS and CMS searches are thus not tailored to them. So far, experiments have focused on $H_0 \to W^+W^-$ [33,34] and $H_0 \to ZZ$ [35,36], or on the search of the CP-odd state via $A_0 \to \tau^+\tau^-$ [37] and $A_0 \to Zh$ [38,39].

The mass ordering of the neutral states in addition to $\alpha \sim \beta$ preferred by a strong EWPT favors the decay $A_0 \to ZH_0$, both due to the large amount of phase space available, and because the coupling $g_{A_0ZH_0} \sim \cos(\alpha-\beta)$ is unsuppressed in the alignment limit. In contrast, the coupling $g_{A_0Zh} \sim \sin(\alpha-\beta)$ vanishes in that limit, and $A_0 \to ZH_0$ even remains dominant over $A_0 \to Zh$ away from alignment (see Fig. 2).

The competing decay channels are $A_0 \to t\bar{t}$ and $A_0 \to W^\pm H^\mp$. The former is suppressed as $(\tan\beta)^{-2}$, which is moderate in our scenario, and is subdominant for $m_{A_0} - m_{H_0} \gtrsim v$ (Fig. 2, top). The latter depends on the splitting $m_{A_0} - m_{H^\pm}$. EW precision observables require $H^\pm$ to be close in mass to either H_0 or A_0 [40], meaning the decay $A_0 \to W^\pm H^\mp$ will be either kinematically forbidden or of similar magnitude to $A_0 \to ZH_0$. Our scan for type I does not prefer one case over the other. For type II, flavor constraints impose $m_{H^\pm} > 360$ GeV at 95% C.L. [41], which disfavors $A_0 \to W^\pm H^\mp$ compared to $A_0 \to ZH_0$ for a strong EWPT. In what follows, we assume for simplicity $m_{H^\pm} \sim m_{A_0}$ (for $m_{H^\pm} \sim m_{H_0}$, the $W^\pm H^\mp$ decay mode would reduce the branching fraction to ZH_0 by a factor of $\sim$2 [32]).

In Fig. 2 (top) we show the main decay branching fractions of A_0 as a function of m_{H_0} for two benchmark points, henceforth referred to as A and B: $m_{A_0} = m_{H^\pm} = 400$ GeV, $\mu = 100$ GeV, $\tan\beta = 2$, with $(\alpha-\beta) = 0.001\pi$ and $(\alpha-\beta) = 0.1\pi$, respectively. We observe that for $m_{A_0} - m_{H_0} \gtrsim v$, $A_0 \to ZH_0$ largely dominates over

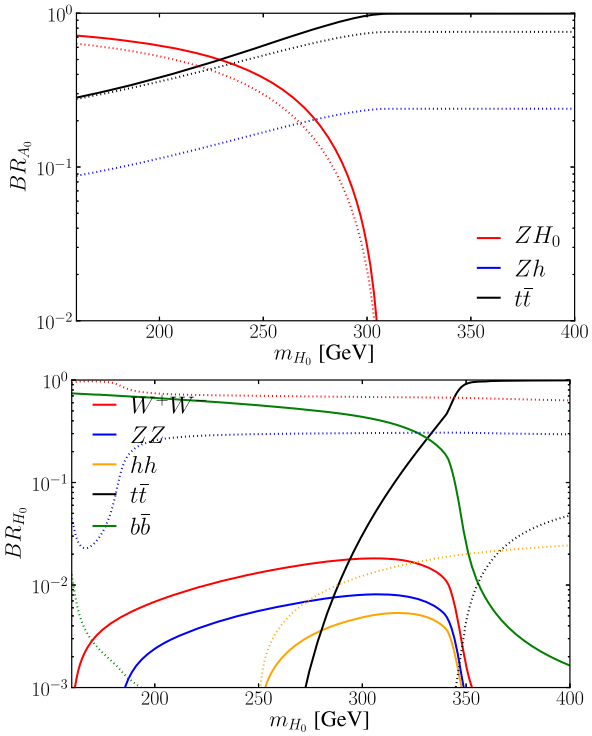

FIG. 2 (color online). Top (bottom): Main branching ratios of the CP-odd (CP-even) scalar A_0 (H_0) as a function of m_{H_0} for $m_{A_0} = m_{H^\pm} = 400$ GeV, $\tan\beta = 2$, $\mu = 100$ GeV, $\alpha - \beta = 0.001\pi$ (solid lines), and $\alpha - \beta = 0.1\pi$ (dotted lines).

$A_0 \to t\bar{t}$ and $A_0 \to Zh$ in both cases. This behavior is even more pronounced as we approach the alignment limit.

As for the subsequent decay of H_0, in the alignment limit the decays $H_0 \to W^+W^-$, $H_0 \to ZZ$, and $H_0 \to hh$ are suppressed, which for the case of a relatively light H_0, as preferred by a strong EWPT (Fig. 1, right), leaves $H_0 \to b\bar{b}$ as the dominant decay mode (Fig. 2, bottom). Moving away from $\alpha = \beta$, the decays into gauge bosons and h become more important, and for $m_{H_0} < 250$ GeV, the decay $H_0 \to W^+W^-$ dominates. For $m_{H_0} \gtrsim 250$ GeV and small μ, this is still the case, while increasing μ enhances the coupling g_{H_0hh} [42] and consequently $H_0 \to hh$.

Consequently, for 2HDMs with a strongly first-order EWPT, the main LHC search channel will either be $pp \to A_0 \to ZH_0 \to \ell\ell b\bar{b}$ or $\ell\ell W^+W^-$, depending on how close the 2HDM is to the alignment limit. These two alternatives are exemplified by our benchmark choices.

Before discussing search prospects in the $\ell\ell b\bar{b}$ and $\ell\ell W^+W^-$ channels at the 14 TeV LHC for these two benchmarks, we remark that these prototypical scenarios generically evade direct H_0 searches. For $\alpha \sim \beta$, $H_0 \to b\bar{b}$ is difficult to extract from the QCD background and the only limits come from $\tau^+\tau^-$ searches. Additionally, with $\alpha > \beta$, and moderate $\tan\beta$, the H_0 coupling to top quarks decreases and direct production of H_0 in gluon fusion gets very suppressed, evading searches in W^+W^- and ZZ channels.

LHC search for A_0 in $\ell\ell b\bar{b}$ and $\ell\ell W^+W^-$.—We now determine the LHC search prospects for the scenario discussed above using simple "cut and count" analyses. We first consider the $\ell\ell b\bar{b}$ final state (see also Ref. [21]). This channel is favored for the nearly aligned benchmark scenario A, for which we choose $m_{H_0} = 180$ GeV. We find that, near alignment, the final state generated via $A_0 \to ZH_0$ largely dominates over $A_0 \to Zh$, which we safely neglect.

The analysis described here was applied to both the 8 and 14 TeV energy stages of the LHC. It was found that the 8 TeV run could potentially observe the process, yielding $S/\sqrt{S+B} \sim 3$ for 20 fb^{-1} of integrated luminosity. This suggests that current LHC data could be sensitive to regions of 2HDM parameter space conducive to a strongly first-order EW phase transition. For example, the analysis in Ref. [43] could be reinterpreted or modified to search for this decay mode. In this Letter, we choose to present the 14 TeV analysis, which permits a clear discovery at the very early stages of the forthcoming run.

The main SM backgrounds to $\ell\ell b\bar{b}$ are (i) QCD semileptonic $t\bar{t}$ production, (ii) $Zb\bar{b}$ production, (iii) ZZ production, and (iv) production of the light Higgs h in association with a Z boson. We implement the type I 2HDM in FEYNRULES [44,45], and use MADGRAPH5_AMC@NLO [46,47] to generate our signal and background analysis samples. These samples are passed to PYTHIA [48] for parton showering and hadronization, and then to DELPHES [49] for detector simulation. We rescale the cross sections for our signal and two dominant backgrounds, $Zb\bar{b}$ and $t\bar{t}$, estimating their respective next-to-leading-order (NLO) values via K factors: $K \simeq 1.6$ for the signal (which we compute using SUSHI [50]), $K \simeq 1.4$ for $Zb\bar{b}$ [51], and $K \simeq 1.5$ for $t\bar{t}$ [52], noting that the remaining backgrounds become negligible upon signal selection.

For event selection, we require the presence of two isolated (within a cone of 0.3) same flavor (SF) leptons in the final state with $P_T^{\ell_1} > 40$, $P_T^{\ell_2} > 20$ and $|\eta_\ell| < 2.5$ (2.7) for electrons (muons), together with two b-tagged [53] jets in the event with $P_T^{b_1} > 40$, $P_T^{b_2} > 20$ and $|\eta_b| < 2.5$. Our analysis is presented in Table I, where the rescaled cross

TABLE I. Event selection (see the section on the decay of $A_0 \to ZH_0$) and background reduction in the $\ell\ell b\bar{b}$ final state. We show the LO cross section (in fb) multiplied by a K factor after successive cuts for the signal $A_0 \to ZH_0 \to \ell\ell b\bar{b}$ and the dominant backgrounds $t\bar{t}$ and $Zb\bar{b}$, while ZZ and $Zh \to \ell\ell b\bar{b}$ are shown at LO.

	Signal	$t\bar{t}$	$Zb\bar{b}$	ZZ	Zh
Event selection	14.6	1578	424	7.3	2.7
$80 < m_{\ell\ell} < 100$ GeV	13.1	240	388	6.6	2.5
$H_T^{bb} > 150$ GeV $H_T^{\ell\ell bb} > 280$ GeV	8.2	57	83	0.8	0.74
$\Delta R_{bb} < 2.5$, $\Delta R_{\ell\ell} < 1.6$	5.3	5.4	28.3	0.75	0.68
m_{bb}, $m_{\ell\ell bb}$ signal region	3.2	1.37	3.2	< 0.01	< 0.02

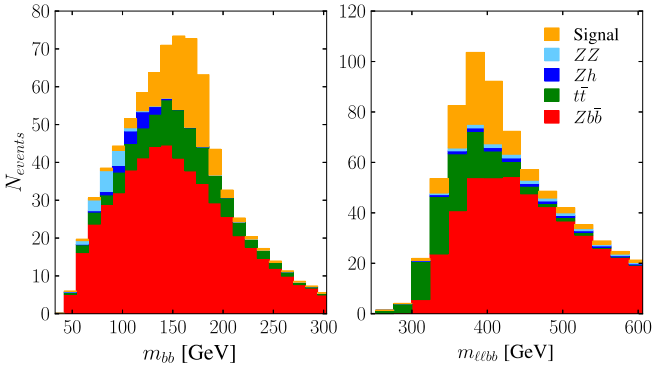

FIG. 3 (color online). m_{bb} (left) and $m_{\ell\ell bb}$ (right) distributions after analysis cuts, with stacked contributions for an integrated luminosity of $\mathcal{L} = 20$ fb^{-1}.

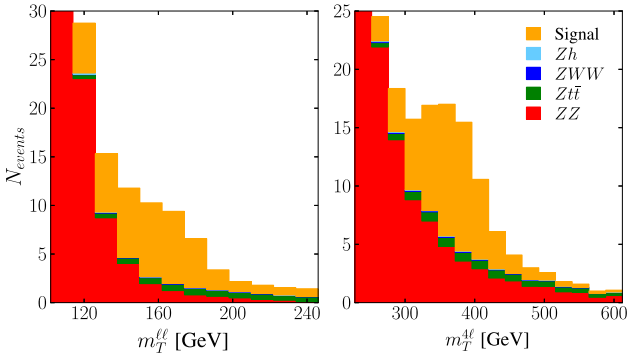

FIG. 4 (color online). $m_T^{\ell\ell}$ (left) and $m_T^{4\ell}$ (right) distributions after event selection, with stacked contributions for an integrated luminosity of $\mathcal{L} = 60$ fb^{-1}.

sections (in fb) for the signal (S) and SM backgrounds (B) are shown after successive cuts. The m_{bb} and $m_{\ell\ell bb}$ invariant mass distributions, after cuts, are shown in Fig. 3, with the contributions stacked for an integrated luminosity of $\mathcal{L} = 20$ fb^{-1}. We define the signal region as $m_{bb} = (m_{H_0} - 20) \pm 30$ GeV and $m_{\ell\ell bb} = (m_{A_0} - 20) \pm 40$ GeV (some energy loss in b jets from showering is expected). Given the results from Table I, we can exclude the background hypothesis with a significance corresponding to 5σ already for $\mathcal{L} \sim 15$ fb^{-1} using the confidence levels method. Marginalizing over a conservative 10% uncertainty in the background predictions yields the same significance with 40 fb^{-1}.

Away from the alignment limit, signal $\ell\ell b\bar{b}$ final states come mostly from $A_0 \to Zh$, since $\mathrm{Br}(H_0 \to b\bar{b}) \ll 1$. Still, for $m_{H_0} \lesssim 250$ GeV the decay $A_0 \to Zh$ is suppressed, which makes the search in this final state challenging. Instead, $A_0 \to ZH_0$ with $H_0 \to WW \to \ell\nu_\ell\ell\nu_\ell$ and $Z \to \ell\ell$ provides the best discovery prospects, as we analyze below for our benchmark B ($H_0 \to ZZ \to \ell\ell q\bar{q}$ is also promising [21], although the required luminosity for discovery is much larger).

The main irreducible SM background to $\ell\ell WW$ with two leptonic W decays is diboson (ZZ) production with $ZZ \to \ell\ell\ell\ell$. Other backgrounds, such as $Zt\bar{t}$, ZWW, and Zh yield a combined cross section which is $< \sigma_{\mathrm{signal}}/4$ after event selection. We follow the same selection and analysis procedure as for the $\ell\ell b\bar{b}$ final state, except for requiring four isolated leptons (in two SF pairs) with $P_T^{\ell_1} > 40$ GeV, $P_T^{\ell_2,\ell_3,\ell_4} > 20$ GeV. We further require one of the SF lepton pairs to reconstruct m_Z within 20 GeV. The leading-order (LO) cross sections at the 14 TeV LHC after event selection for the signal, ZZ background, and the combined rare backgrounds ($Zt\bar{t}$, ZWW, and Zh) are, respectively, 0.93, 5.6, and 0.25 fb (a $\Delta R_{\ell\ell}$ cut or a Z veto on the remaining SF lepton pair would further suppress the ZZ background if necessary). We rescale the signal and dominant background by their respective NLO K factors (1.35 for $Zt\bar{t}$ [55] and 1.2 for ZZ [56]). Defining the transverse mass variables $m_T^{\ell\ell}$ and $m_T^{4\ell}$

$$(m_T^{\ell\ell})^2 = \left(\sqrt{p_{T,\ell\ell}^2 + m_{\ell\ell}^2} + \not{p}_T\right)^2 - (\vec{p}_{T,\ell\ell} + \vec{\not{p}}_T)^2$$

$$m_T^{4\ell} = \sqrt{p_{T,\ell'\ell'}^2 + m_{\ell'\ell'}^2} + \sqrt{p_{T,\ell\ell}^2 + (m_T^{\ell\ell})^2}$$

($\ell'\ell'$ are the two SF leptons most closely reconstructing m_Z), a signal region of $m_T^{4\ell} > 260$ GeV (see Fig. 4) extracts a clean signal without further selection, allowing for the reconstruction of the two masses. A final signal cross section of 0.88 fb compared to a background of 1.39 fb reaches a significance of 5σ with $\mathcal{L} \sim 60$ fb^{-1}, which increases to 200 fb^{-1} when assuming a 10% systematic uncertainty on the background prediction.

Discussion and outlook.—Uncovering the structure of the SM scalar sector will be a central task for the LHC in the coming years. This will have important implications for our understanding of electroweak symmetry breaking and possibly for open cosmological problems such as the origin of visible matter. Extensions of the SM scalar sector that address these questions may yield distinctive signatures at the LHC. We have shown in this Letter that the decay $A_0 \to ZH_0$ is a "smoking gun" signature of 2HDM scenarios with a strongly first-order electroweak phase transition, that could explain the origin of the matter-antimatter asymmetry in the Universe. We claim that current 8 TeV LHC data may be sensitive to this decay in the $\ell\ell b\bar{b}$ channel. Furthermore, we demonstrate that search prospects for these scenarios at the 14 TeV run in both the previous channel as well as $\ell\ell WW \to \ell\ell\ell\ell\nu\nu$ are very promising, with a discovery of the new scalar states A_0 and H_0 possible with $\mathcal{L} \sim 15$–40 and 60–200 fb^{-1} respectively, thus providing a probe of electroweak cosmology at the LHC.

We thank V. Sanz, M. Ramsey-Musolf, and S. Su for useful discussions and comments. S. J. H. and K. M. are supported by the Science Technology and Facilities Council (STFC) under Grant No. ST/J000477/1. J. M. N. is supported by the People Programme (Marie Curie

Actions) of the European Union's Seventh Framework Programme (FP7/2007-2013) under Grant agreement No. PIEF-GA-2013-625809. G. C. D. is supported by the Coordenação de Aperfeiçoamento de Pessoal de Nível Superior (CAPES-Brazil) under Grant No. 0963/13-5.

[1] ATLAS Collaboration, Phys. Lett. B **716**, 1 (2012).
[2] CMS Collaboration, Phys. Lett. B **716**, 30 (2012).
[3] A. Djouadi, Phys. Rep. **459**, 1 (2008).
[4] J. Mrazek, A. Pomarol, R. Rattazzi, M. Redi, J. Serra, and A. Wulzer, Nucl. Phys. **B853**, 1 (2011).
[5] E. Bertuzzo, T. S. Ray, H. de Sandes, and C. A. Savoy, J. High Energy Phys. 05 (2013) 153.
[6] N. Turok and J. Zadrozny, Nucl. Phys. **B358**, 471 (1991).
[7] J. M. Cline, K. Kainulainen, and A. P. Vischer, Phys. Rev. D **54**, 2451 (1996).
[8] L. Fromme, S. J. Huber, and M. Seniuch, J. High Energy Phys. 11 (2006) 038.
[9] J. M. Cline, K. Kainulainen, and M. Trott, J. High Energy Phys. 11 (2011) 089.
[10] J. Shu and Y. Zhang, Phys. Rev. Lett. **111**, 091801 (2013).
[11] T. A. Chowdhury, M. Nemevsek, G. Senjanovic, and Y. Zhang, J. Cosmol. Astropart. Phys. 02 (2012) 029.
[12] G. C. Branco, P. M. Ferreira, L. Lavoura, M. N. Rebelo, M. Sher, and J. P. Silva, Phys. Rep. **516**, 1 (2012).
[13] A. Celis, V. Ilisie, and A. Pich, J. High Energy Phys. 07 (2013) 053.
[14] M. Krawczyk, D. Sokolowska, and B. Swiezewska, J. Phys. Conf. Ser. **447**, 012050 (2013).
[15] B. Grinstein and P. Uttayarat, J. High Energy Phys. 06 (2013) 094; 09 (2013) 110.
[16] C.-Y. Chen, S. Dawson, and M. Sher, Phys. Rev. D **88**, 015018 (2013).
[17] N. Craig, J. Galloway, and S. Thomas, arXiv:1305.2424.
[18] O. Eberhardt, U. Nierste, and M. Wiebusch, J. High Energy Phys. 07 (2013) 118.
[19] S. Kanemura, S. Moretti, Y. Mukai, R. Santos, and K. Yagyu, Phys. Rev. D **79**, 055017 (2009).
[20] J. Baglio, O. Eberhardt, U. Nierste, and M. Wiebusch, Phys. Rev. D **90**, 015008 (2014).
[21] B. Coleppa, F. Kling, and S. Su, J. High Energy Phys. 09 (2014) 161.
[22] G. C. Dorsch, S. J. Huber, and J. M. No, J. High Energy Phys. 10 (2013) 029.
[23] S. L. Glashow and S. Weinberg, Phys. Rev. D **15**, 1958 (1977).
[24] D. Eriksson, J. Rathsman, and O. Stal, Comput. Phys. Commun. **181**, 189 (2010).
[25] P. Bechtle, O. Brein, S. Heinemeyer, O. Stl, T. Stefaniak, G. Weiglein, and K. E. Williams, Eur. Phys. J. C **74**, 2693 (2014).
[26] I. F. Ginzburg and I. P. Ivanov, Phys. Rev. D **72**, 115010 (2005).
[27] F. Mahmoudi and O. Stal, Phys. Rev. D **81**, 035016 (2010).
[28] G. D. Moore, Phys. Rev. D **59**, 014503 (1998).
[29] M. Quiros, Helv. Phys. Acta **67**, 451 (1994).
[30] P. B. Arnold and O. Espinosa, Phys. Rev. D **47**, 3546 (1993); **50**, E6662 (1994).
[31] Z. Fodor and A. Hebecker, Nucl. Phys. **B432**, 127 (1994).
[32] G. C. Dorsch, S. Huber, K. Mimasu, and J. M. No (to be published).
[33] ATLAS Collaboration, Report No. ATLAS-CONF-2013-027.
[34] ATLAS Collaboration, Report No. ATLAS-CONF-2013-067.
[35] ATLAS Collaboration, Report No. ATLAS-CONF-2013-013.
[36] CMS Collaboration, Report No. CMS-PAS-HIG-12-024.
[37] ATLAS Collaboration, Report No. ATLAS-CONF-2012-094.
[38] CMS Collaboration, Report No. CMS-PAS-HIG-13-025.
[39] ATLAS Collaboration, Report No. ATL-PHYS-PUB-2013-016.
[40] W. Grimus, L. Lavoura, O. M. Ogreid, and P. Osland, J. Phys. G **35**, 075001 (2008); Nucl. Phys. **B801**, 81 (2008).
[41] T. Hermann, M. Misiak, and M. Steinhauser, J. High Energy Phys. 11 (2012) 036.
[42] S. Kanemura, Y. Okada, E. Senaha, and C.-P. Yuan, Phys. Rev. D **70**, 115002 (2004).
[43] ATLAS Collaboration, Report No. ATLAS-CONF-2013-079.
[44] N. D. Christensen and C. Duhr, Comput. Phys. Commun. **180**, 1614 (2009).
[45] C. Degrande, C. Duhr, B. Fuks, D. Grellscheid, O. Mattelaer, and T. Reiter, Comput. Phys. Commun. **183**, 1201 (2012).
[46] J. Alwall, M. Herquet, F. Maltoni, O. Mattelaer, and T. Stelzer, J. High Energy Phys. 06 (2011) 128.
[47] J. Alwall, R. Frederix, S. Frixione, V. Hirschi, F. Maltoni, O. Mattelaer, H.-S. Shao, T. Stelzer, P. Torrielli, and M. Zaro, J. High Energy Phys. 07 (2014) 079.
[48] T. Sjostrand, S. Mrenna, and P. Z. Skands, Comput. Phys. Commun. **178**, 852 (2008).
[49] J. de Favereau, C. Delaere, P. Demin, A. Giammanco, V. Lemaître, A. Mertens, and M. Selvaggi, J. High Energy Phys. 02 (2014) 057.
[50] R. V. Harlander, S. Liebler, and H. Mantler, Comput. Phys. Commun. **184**, 1605 (2013).
[51] J. M. Campbell, R. K. Ellis, F. Maltoni, and S. Willenbrock, Phys. Rev. D **73**, 054007 (2006); **77**, 019903(E) (2008).
[52] M. L. Mangano, P. Nason, and G. Ridolfi, Nucl. Phys. **B373**, 295 (1992); G. Bevilacqua, M. Czakon, A. van Hameren, C. G. Papadopoulos, and M. Worek, J. High Energy Phys. 02 (2011) 083.
[53] We estimate the kinematical dependence of the b-tagging efficiency from a recent CMS Collaboration performance note [54]. Our acceptance region is divided into (η, P_T) categories according to Fig. 15 of Ref. [54]. The efficiency imposed on a jet belonging to a given category is obtained as the average of the η and P_T bins, whose values range between 60%–70%.
[54] CMS Collaboration, Report No. CMS-PAS-BTV-13-001.
[55] A. Lazopoulos, T. McElmurry, K. Melnikov, and F. Petriello, Phys. Lett. B **666**, 62 (2008).
[56] J. Ohnemus, Phys. Rev. D **50**, 1931 (1994).